European Congress on Computational Methods
in Applied Sciences and Engineering (ECCOMAS 2012)
J. Eberhardsteiner et.al. (eds.)
Vienna, Austria, September 10-14, 2012

A GEOMETRIC BRIDGE BETWEEN REGULARISED DAMAGE AND ENERGETICALLY EQUIVALENT CRACKS

Elena Tamayo-Mas, Antonio Rodríguez-Ferran

Laboratori de Càlcul Numèric (LaCàN)
Universitat Politècnica de Catalunya (UPC)
Campus Nord UPC, 08034 Barcelona, Spain
e-mail: {elena.tamayo, antonio.rodriguez-ferran}@upc.edu

Keywords: gradient damage, regularisation, smoothed displacements, cohesive cracks, energy balance, medial axis

Abstract. *In order to achieve a better characterisation of a whole failure process, models which combine damage and fracture mechanics have recently been proposed. Here, a new combined methodology is presented: in order to describe damage inception and its diffuse propagation, a gradient-enhanced continuum model based on smoothed displacements is used, which is coupled to a discontinuous one to describe the final stages of the process.*
Special emphasis should be placed on the difficulties concerning the transition between continuous damage growth and fracture. On the one hand, and in order to conserve the energy dissipation through the change of models, an appropriate cohesive law must be defined. In this paper, the proposed technique to define this law is explained. On the other hand, the direction of the crack path should be determined. Here, a new strategy is proposed: the discontinuity is propagated following the direction dictated by the medial axis of the damaged domain. That is, a geometric tool, widely used in the computer graphics field, is used here to locate cracks.

1 INTRODUCTION

Simulation of failure of quasi-brittle materials requires either the description of strain localisation and the accumulation of damage or the possible formation of propagating cracks. In order to deal with all these features, damage and fracture mechanics are the two typically used approaches. The former, which belongs to the family of continuous models, is able to capture damage inception and its diffuse propagation [1]. The latter, which falls in the family of discontinuous models, can be used to model the final stages of failure processes, when the body is physically separated in two or more parts. Nevertheless, damage models cannot deal with material separation, while discontinuous models cannot be used for modelling neither damage formation nor its diffuse propagation [2].

As suggested by the above paragraph, in order to achieve a better characterisation of the whole failure process, integrated strategies which combine these two traditional approaches may be employed. These continuous-discontinuous strategies are characterised by the following features:

- In order to describe the first stages of the failure process, damage models are used. As shown in [3] these approaches are characterised by a strain softening phenomenon, which leads to a physically unrealistic treatment of the energy dissipated during the failure process. Therefore, combined approaches use any of the solutions proposed in the literature, see [4] for details, to overcome this physically unrealistic behaviour thus leading to numerical simulations that do not present mesh sensitivity.

- At the end of each time step, the approach checks if the transition criterion is fulfilled. In such a case, a discrete cohesive crack is introduced into the model and the direction of its propagation is determined. In order to characterise these propagating discontinuities, different techniques, mainly based on the cohesive crack concept [5], have been developed. From a numerical viewpoint, their applications were first restricted, since the standard finite element method (FEM), which performs well approximating smooth functions, is not suited for the approximation of non-smooth solutions. Therefore, as reviewed in [6], special techniques have to be used to deal with propagating cracks. Among these special methods, the eXtended Finite Element Method (X-FEM) [7, 8] is the most employed.

- From that moment on, a discontinuous approach is used to model the final stages of the failure process. Therefore, the numerical interaction between the separated parts of the body ceases and realistic results may be obtained.

In the computational mechanics community, different integrated strategies have been proposed. In [9], the combination of the smeared and embedded descriptions of cracking is analysed. Traction-free discontinuities are coupled to a softening viscoplastic bulk and to a gradient-enhanced continuum damage model in [10] and [11] respectively. In [12], the non-local continuum damage approach used for modelling the early steps of failure process is coupled to a cohesive crack model in order to describe the final stages of failure.

This paper addresses a new contribution in this direction, see Figure 1. In order to obtain an objective description of the first stages of the failure process, a regularised damage model is employed. Here, a formulation with regularised displacements is employed in order to obtain physically realistic results. For the sake of simplicity, only elastic-scalar gradient damage models are considered. However, smoothed displacements can be used either in an integral or in a

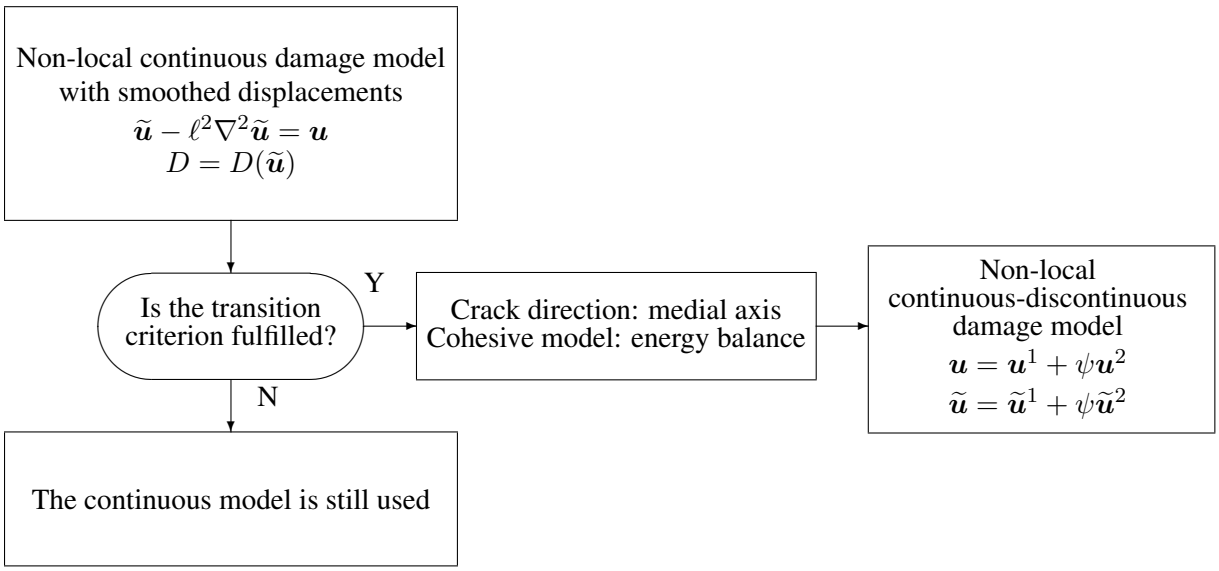

Figure 1: Proposed continuous-discontinuous model.

gradient version, as originally proposed by [13], and may be extended to other models such as plasticity, as presented in [14].

When the transition criterion is fulfilled, the coupling to a discontinuous strategy is carried out, thus introducing a propagating crack described by a cohesive law. The discontinuity is propagated following the direction dictated by the $\theta-$simplified medial axis of the already damaged domain. Therefore, the geometric criterion introduced by [15], which is widely used in the computer graphics field, is used here to locate propagating cracks. The cohesive law is defined through an energy balance in order to conserve the energy dissipation through the change of models.

1.1 Outline

An outline of this paper follows. The new continuous-discontinuous model is presented in section 2. Section 3 deals with two important issues concerning the transition from the continuum to the discrete strategy: the definition of the cohesive law (section 3.1) and the determination of the crack path (section 3.2). The capabilities of this new technique to locate cracks are illustrated by means of a benchmark test in section 4. The concluding remarks of section 5 close the paper.

2 MODEL FORMULATION

2.1 Discontinuous displacements

Consider the domain Ω bounded by $\Gamma = \Gamma_u \cup \Gamma_t \cup \Gamma_d$, as shown in Figure 2. Prescribed displacements are imposed on Γ_u, prescribed tractions are imposed on Γ_t and the boundary Γ_d consists of the boundary of the crack.

Then, and by means of the X-FEM, the standard $\boldsymbol{u}$ and the auxiliary displacement field $\widetilde{\boldsymbol{u}}$ can be decomposed as

$$\boldsymbol{u}(\boldsymbol{x}) = \boldsymbol{u}^1(\boldsymbol{x}) + \psi(\boldsymbol{x})\,\boldsymbol{u}^2(\boldsymbol{x}) \qquad \text{in } \bar{\Omega} = \Omega \cup \Gamma \tag{1}$$

$$\widetilde{\boldsymbol{u}}(\boldsymbol{x}) = \widetilde{\boldsymbol{u}}^1(\boldsymbol{x}) + \psi(\boldsymbol{x})\,\widetilde{\boldsymbol{u}}^2(\boldsymbol{x}) \qquad \text{in } \bar{\Omega} = \Omega \cup \Gamma \tag{2}$$

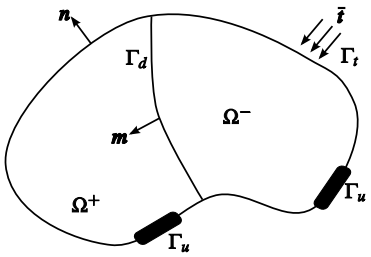

Figure 2: Notations for a body with a crack subjected to loads and imposed displacements.

where $\boldsymbol{u}^i(\boldsymbol{x})$, $\widetilde{\boldsymbol{u}}^i(\boldsymbol{x})$ $(i=1,2)$ are continuous fields and $\psi(\boldsymbol{x})$ is the enrichment function (e.g. the sign function) centred at Γ_d.

2.2 Governing equations

The strong form of the equilibrium equation and boundary conditions for the body $\bar{\Omega}$ without body forces is given by

$$\nabla \cdot \boldsymbol{\sigma} = \mathbf{0} \quad \text{in } \Omega \tag{3}$$
$$\boldsymbol{\sigma} \cdot \boldsymbol{n} = \bar{\boldsymbol{t}} \quad \text{on } \Gamma_t \tag{4}$$
$$\boldsymbol{\sigma} \cdot \boldsymbol{m} = \bar{\boldsymbol{t}}_d \quad \text{on } \Gamma_d \tag{5}$$
$$\boldsymbol{u} = \boldsymbol{u}^* \quad \text{on } \Gamma_u \tag{6}$$

where $\boldsymbol{\sigma}$ is the Cauchy stress tensor, $\boldsymbol{u}^*$ is a prescribed displacement, $\bar{\boldsymbol{t}}$ is the load on the boundary and $\bar{\boldsymbol{t}}_d$ is the load on the discontinuity surface. Note that $\boldsymbol{n}$ is the outward unit normal to the body and $\boldsymbol{m}$ is the inward unit normal to Ω^+ on Γ_d, see Figure 2.

To complete the strong form of the mechanical problem, an isotropic damage model

$$\boldsymbol{\sigma}(\boldsymbol{x}) = [1 - D(\boldsymbol{x})]\, \boldsymbol{C} : \boldsymbol{\varepsilon}(\boldsymbol{x}) \tag{7}$$

is considered, where $\boldsymbol{\varepsilon}(\boldsymbol{x}) = \nabla^s \boldsymbol{u}(\boldsymbol{x})$ is the small strain tensor, $\boldsymbol{C}$ is the fourth-order tensor of elastic moduli and D is the isotropic damage parameter ($0 \leq D \leq 1$ and $\dot{D} \geq 0$).

In order to regularise the problem, the second-order diffusion partial differential equation

$$\widetilde{\boldsymbol{u}} - \ell^2 \nabla^2 \widetilde{\boldsymbol{u}}(\boldsymbol{x}) = \boldsymbol{u}(\boldsymbol{x}) \qquad \text{in } \Omega \setminus \Gamma_d \tag{8}$$

is coupled with the mechanical equations. Both for the standard and the enhanced displacement fields, combined boundary conditions

$$\left.\begin{array}{rcl} \widetilde{\boldsymbol{u}}^i \cdot \boldsymbol{n} & = & \boldsymbol{u}^i \cdot \boldsymbol{n} \\ \nabla(\widetilde{\boldsymbol{u}}^i \cdot \boldsymbol{t}) \cdot \boldsymbol{n} & = & \nabla(\boldsymbol{u}^i \cdot \boldsymbol{t}) \cdot \boldsymbol{n} \end{array}\right\} \text{on } \Gamma \qquad \left.\begin{array}{rcl} \widetilde{\boldsymbol{u}}^i \cdot \boldsymbol{m} & = & \boldsymbol{u}^i \cdot \boldsymbol{m} \\ \nabla(\widetilde{\boldsymbol{u}}^i \cdot \boldsymbol{t}) \cdot \boldsymbol{m} & = & \nabla(\boldsymbol{u}^i \cdot \boldsymbol{t}) \cdot \boldsymbol{m} \end{array}\right\} \text{on } \Gamma_d \tag{9}$$

where $i = 1, 2$, are proposed: Dirichlet boundary conditions are prescribed for the normal component of the displacement field whereas non-homogeneous Neumann boundary conditions are imposed for the tangential one. These combined conditions satisfy the necessary properties for regularisation, see [16] for details: (a) reproducibility of order 1 ($\boldsymbol{u} = \widetilde{\boldsymbol{u}}$ if $\boldsymbol{u}$ is a linear field), (b) displacement smoothing along the boundary and (c) volume preservation.

2.3 Variational formulation

The space of trial standard displacements is characterised by the function defined in Eq. (1), where

$$\boldsymbol{u}^1, \boldsymbol{u}^2 \in \mathcal{U}_{\boldsymbol{u}} = \left\{ \boldsymbol{u} \mid \boldsymbol{u} \in H^1(\Omega) \text{ and } \boldsymbol{u}_{|\Gamma_u} = \boldsymbol{u}^* \right\} \tag{10}$$

with $H^1(\Omega)$ a Sobolev space. Analogously, the space of admissible displacement variations is defined by the weight function $\boldsymbol{\omega}(\boldsymbol{x}) = \boldsymbol{\omega}^1(\boldsymbol{x}) + \psi(\boldsymbol{x})\boldsymbol{\omega}^2(\boldsymbol{x})$ with

$$\boldsymbol{\omega}^1, \boldsymbol{\omega}^2 \in \mathcal{W}_{\boldsymbol{u},\boldsymbol{0}} = \left\{ \boldsymbol{\omega} \mid \boldsymbol{\omega} \in H^1(\Omega) \text{ and } \boldsymbol{\omega}_{|\Gamma_u} = \boldsymbol{0} \right\} \tag{11}$$

Following standard procedures, the equilibrium Eq. (3) can be cast in a variational form, thus leading to

$$\int_\Omega \nabla^s \boldsymbol{\omega}^1 : \boldsymbol{\sigma} \, \mathrm{d}\Omega = \int_{\Gamma_t} \boldsymbol{\omega}^1 \cdot \bar{\boldsymbol{t}} \, \mathrm{d}\Gamma \qquad \forall \boldsymbol{\omega}^1 \in H^1(\Omega) \tag{12}$$

$$\int_\Omega \psi \nabla^s \boldsymbol{\omega}^2 : \boldsymbol{\sigma} \, \mathrm{d}\Omega + 2\int_{\Gamma_d} \boldsymbol{\omega}^2 \cdot \bar{\boldsymbol{t}}_d \, \mathrm{d}\Gamma = \int_{\Gamma_t} \psi \boldsymbol{\omega}^2 \cdot \bar{\boldsymbol{t}} \, \mathrm{d}\Gamma \qquad \forall \boldsymbol{\omega}^2 \in H^1(\Omega) \tag{13}$$

where at the discontinuity Γ_d,

$$\dot{\bar{\boldsymbol{t}}}_d = f\left([\![\dot{\boldsymbol{u}}]\!] \right) \tag{14}$$

with f relating traction rate $\dot{\bar{\boldsymbol{t}}}_d$ and displacement jump rate $[\![\dot{\boldsymbol{u}}]\!]$.

Similarly to the equilibrium equation, the regularisation PDE (8) is also cast in a weak form. Characterising the space of trial smoothed displacements $\widetilde{\boldsymbol{u}}$ by the function defined in Eq. (2), with $\boldsymbol{u}^1, \boldsymbol{u}^2 \in \mathcal{U}_{\boldsymbol{u}}$, one obtains

$$\begin{aligned} \int_\Omega \boldsymbol{\omega}^1 \cdot (\widetilde{\boldsymbol{u}}^1 + \psi \widetilde{\boldsymbol{u}}^2) \, \mathrm{d}\Omega + \ell^2 \int_\Omega \nabla \boldsymbol{\omega}^1 : \left(\nabla \widetilde{\boldsymbol{u}}^1 + \psi \nabla \widetilde{\boldsymbol{u}}^2 \right) \mathrm{d}\Omega + 2\ell^2 \int_{\Gamma_d} \omega_t^1 \left(\nabla \left(\boldsymbol{u}^2 \cdot \boldsymbol{t} \right) \cdot \boldsymbol{m} \right) \mathrm{d}\Gamma = \\ = \int_\Omega \boldsymbol{\omega}^1 \cdot (\boldsymbol{u}^1 + \psi \boldsymbol{u}^2) \, \mathrm{d}\Omega + \ell^2 \int_{\Gamma \setminus \Gamma_d} \omega_t^1 \left(\nabla \left(\boldsymbol{u}^1 \cdot \boldsymbol{t} \right) \cdot \boldsymbol{n} + \psi \nabla \left(\boldsymbol{u}^2 \cdot \boldsymbol{t} \right) \cdot \boldsymbol{n} \right) \mathrm{d}\Gamma \end{aligned} \tag{15}$$

$$\begin{aligned} \int_\Omega \boldsymbol{\omega}^2 \cdot (\psi \widetilde{\boldsymbol{u}}^1 + \widetilde{\boldsymbol{u}}^2) \, \mathrm{d}\Omega + \ell^2 \int_\Omega \nabla \boldsymbol{\omega}^2 : \left(\psi \nabla \widetilde{\boldsymbol{u}}^1 + \nabla \widetilde{\boldsymbol{u}}^2 \right) \mathrm{d}\Omega + 2\ell^2 \int_{\Gamma_d} \omega_t^2 \left(\nabla \left(\boldsymbol{u}^1 \cdot \boldsymbol{t} \right) \cdot \boldsymbol{m} \right) \mathrm{d}\Gamma = \\ = \int_\Omega \boldsymbol{\omega}^2 \cdot (\psi \boldsymbol{u}^1 + \boldsymbol{u}^2) \, \mathrm{d}\Omega + \ell^2 \int_{\Gamma \setminus \Gamma_d} \omega_t^2 \left(\psi \nabla \left(\boldsymbol{u}^1 \cdot \boldsymbol{t} \right) \cdot \boldsymbol{n} + \nabla \left(\boldsymbol{u}^2 \cdot \boldsymbol{t} \right) \cdot \boldsymbol{n} \right) \mathrm{d}\Gamma \end{aligned} \tag{16}$$

$\forall \boldsymbol{\omega}^1, \boldsymbol{\omega}^2 \in \mathcal{W}_{\boldsymbol{u},\boldsymbol{0}}$.

2.4 Finite element discretisation

Employing an extended finite element strategy to prevent remeshing and other kinds of techniques, Eq. (1) and (2) read, in the domain of an element with enhanced nodes,

$$\mathbf{u}(\boldsymbol{x}) = \mathbf{N}(\boldsymbol{x})\mathbf{u}^1 + \psi(\boldsymbol{x})\mathbf{N}(\boldsymbol{x})\mathbf{u}^2 \tag{17}$$

$$\widetilde{\mathbf{u}}(\boldsymbol{x}) = \mathbf{N}(\boldsymbol{x})\widetilde{\mathbf{u}}^1 + \psi(\boldsymbol{x})\mathbf{N}(\boldsymbol{x})\widetilde{\mathbf{u}}^2 \tag{18}$$

where $\mathbf{N}$ is the matrix of standard finite element shape functions, $\mathbf{u}^1$, $\widetilde{\mathbf{u}}^1$ are the basic nodal degrees of freedom and $\mathbf{u}^2$, $\widetilde{\mathbf{u}}^2$ are the enhanced ones. The discrete format of the problem fields leads to the four discrete weak governing equations

$$\int_\Omega \mathbf{B}^T \boldsymbol{\sigma} \, \mathrm{d}\Omega \;\; = \;\; \int_{\Gamma_t} \mathbf{N}^T \bar{\boldsymbol{t}} \, \mathrm{d}\Gamma \tag{19}$$

$$\int_\Omega \psi \mathbf{B}^T \boldsymbol{\sigma}\,\mathrm{d}\Omega + 2\int_{\Gamma_d} \mathbf{N}^T \bar{\boldsymbol{t}}_d\,\mathrm{d}\Gamma = \int_{\Gamma_t} \psi \mathbf{N}^T \bar{\boldsymbol{t}}\,\mathrm{d}\Gamma \tag{20}$$

$$(\mathbf{M}+\ell^2\mathbf{D})\widetilde{\mathbf{u}}^1 + (\mathbf{M}_\psi+\ell^2\mathbf{D}_\psi)\widetilde{\mathbf{u}}^2 = (\mathbf{M}+\ell^2\boldsymbol{C}^{\Gamma\setminus\Gamma_d,\boldsymbol{n}})\mathbf{u}^1 + (\mathbf{M}_\psi+\ell^2(\boldsymbol{C}_\psi^{\Gamma\setminus\Gamma_d,\boldsymbol{n}} - 2\boldsymbol{C}^{\Gamma_d,\boldsymbol{m}}))\mathbf{u}^2 \tag{21}$$

$$(\mathbf{M}_\psi+\ell^2\mathbf{D}_\psi)\widetilde{\mathbf{u}}^1 + (\mathbf{M}+\ell^2\mathbf{D})\widetilde{\mathbf{u}}^2 = (\mathbf{M}_\psi+\ell^2(\boldsymbol{C}_\psi^{\Gamma\setminus\Gamma_d,\boldsymbol{n}} - 2\boldsymbol{C}^{\Gamma_d,\boldsymbol{m}}))\mathbf{u}^1 + (\mathbf{M}+\ell^2\boldsymbol{C}^{\Gamma\setminus\Gamma_d,\boldsymbol{n}})\mathbf{u}^2 \tag{22}$$

where $\mathbf{B}$ is the matrix of shape function derivatives and

$$\mathbf{M} = \int_\Omega \mathbf{N}^T\mathbf{N}\,\mathrm{d}\Omega \qquad \mathbf{D} = \int_\Omega \nabla\mathbf{N}^T\nabla\mathbf{N}\,\mathrm{d}\Omega \tag{23}$$

$$\mathbf{M}_\psi = \int_\Omega \psi\mathbf{N}^T\mathbf{N}\,\mathrm{d}\Omega \qquad \mathbf{D}_\psi = \int_\Omega \psi\nabla\mathbf{N}^T\nabla\mathbf{N}\,\mathrm{d}\Omega \tag{24}$$

$$\boldsymbol{C}^{\Gamma,\boldsymbol{n}} = \int_\Gamma \mathbf{N}^T\boldsymbol{t}\boldsymbol{t}^T\left[\frac{\partial\mathbf{N}}{\partial x}n_x + \frac{\partial\mathbf{N}}{\partial y}n_y\right]\mathrm{d}\Gamma \qquad \boldsymbol{C}_\psi^{\Gamma,\boldsymbol{n}} = \int_\Gamma \psi\mathbf{N}^T\boldsymbol{t}\boldsymbol{t}^T\left[\frac{\partial\mathbf{N}}{\partial x}n_x + \frac{\partial\mathbf{N}}{\partial y}n_y\right]\mathrm{d}\Gamma \tag{25}$$

Some remarks about the discretisation:

- Eq. (19) is the standard non-linear system of equilibrium equations, while Eq. (20) deals with the contribution of the crack, which is multiplied by a factor of two due to the fact that the enrichment function is the sign function ($\psi\psi = +1$).
- Matrices $\mathbf{M}$ and $\mathbf{D}$ are the constant mass and diffusivity matrices already obtained in [13]. The enriched matrices $\mathbf{M}_\psi$ and $\mathbf{D}_\psi$ are also constant, once the finite element is cracked.
- Matrices $\boldsymbol{C}^{\Gamma\setminus\Gamma_d,\boldsymbol{n}}$, $\boldsymbol{C}_\psi^{\Gamma\setminus\Gamma_d,\boldsymbol{n}}$ and $\boldsymbol{C}^{\Gamma_d,\boldsymbol{m}}$ contain contributions from the combined boundary conditions, Eq. (9). Since Dirichlet boundary conditions are prescribed for the normal component of the displacement field on Γ, the normal component of the weight function $\boldsymbol{\omega}$ vanishes on the boundary thus leading to

$$\int_\Gamma \boldsymbol{\omega}\nabla\widetilde{\boldsymbol{u}}\cdot\boldsymbol{n}\,\mathrm{d}\Gamma = \int_\Gamma \omega_t\nabla(\widetilde{\boldsymbol{u}}\cdot\boldsymbol{t})\cdot\boldsymbol{n}\,\mathrm{d}\Gamma = \int_\Gamma \omega_t\nabla(\boldsymbol{u}\cdot\boldsymbol{t})\cdot\boldsymbol{n}\,\mathrm{d}\Gamma \tag{26}$$

  Again, $\boldsymbol{C}^{\Gamma_d,\boldsymbol{m}}$ is multiplied by a factor of two because of the sign function.

3 TRANSITION

When dealing with the transition from a continuous model to a discontinuous approach, different issues concerning the properties of the crack should be defined. Here, special emphasis is placed on two of these issues. On the one hand, the technique to define the cohesive law is explained. On the other hand, the proposed strategy to determine the crack direction is presented.

3.1 Cohesive model

When introducing a discontinuity in the bulk, the properties of the cohesive crack should be defined. The strategy here used is based on the idea that the energy which would be dissipated by a continuum approach is conserved if a combined strategy is used, see [12, 20].

Consider first the continuous approach and a damaged band λ_D. Then, in this zone of the structure, the dissipated energy can be expressed as

$$\Psi_C = \int_{\lambda_D} \psi_C\,\mathrm{d}\Omega = \int_{\lambda_D}\int_0^{t_f} \boldsymbol{\sigma}_C\cdot\dot{\boldsymbol{\varepsilon}}_C\,\mathrm{d}t\,\mathrm{d}\Omega \tag{27}$$

where the subscript C stands for *Continuous strategy* and $\dot{\boldsymbol{\varepsilon}}_C$ is the strain rate tensor.

Consider now the combined approach. In λ_D, the dissipated energy can be decomposed into two contributions

$$\Psi_{CD} = \Psi_{CD}^{\text{bulk}} + \Psi_{CD}^{\text{crack}} = \int_{\lambda_D} \int_0^{t_f} \boldsymbol{\sigma}_{CD} \cdot \dot{\boldsymbol{\varepsilon}}_{CD} \, \mathrm{d}t \, \Omega + \Psi_{CD}^{\text{crack}} \tag{28}$$

where the subscript CD stands for *Continuous-Discontinuous strategy*, Ψ_{CD}^{bulk} is the dissipated energy of the bulk and Ψ_{CD}^{crack} is the fracture energy.

Hence, imposing energy balance

$$\Psi_C = \Psi_{CD}, \tag{29}$$

see Figure 3, the fracture energy

$$\Psi_{CD}^{\text{crack}} = \Psi_C - \Psi_{CD}^{\text{bulk}} \tag{30}$$

is computed and can be transferred to the crack at the moment of the transition.

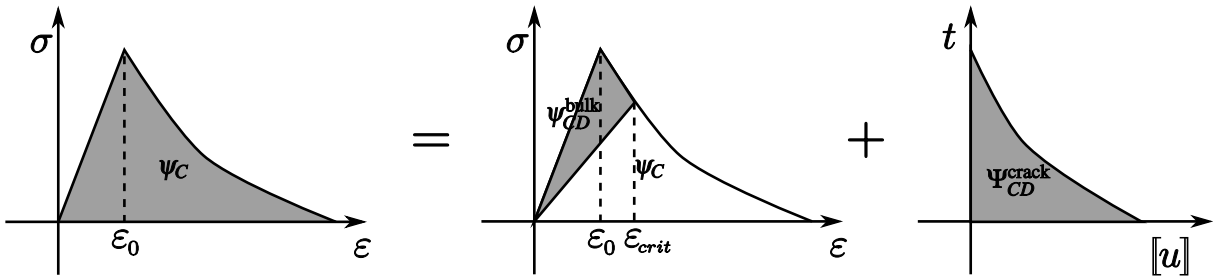

Figure 3: Energy balance.

In order to estimate the fracture energy, different techniques can be employed. In [12], an analytical estimation of Ψ_{CD}^{crack}, and thus, of the crack stiffness, is computed. Nevertheless, with this procedure, the fracture energy is overestimated. Indeed, by means of these assumptions, in all points across the damage band λ_D, the energy $\Psi_C - \Psi_{CD}^{\text{bulk}}$ depicted in Figure 4a is transferred to the crack. However, in some of these points, the continuous strategy would dissipate less energy, see Figure 4b.

As suggested by this discussion, we propose to employ a new methodology which takes into account, for each point across the damage band λ_D, the unloading behaviour (both softening and secant) of the continuous bulk. Since the continuous unloading branch is only known up to the activation of the continuous-discontinuous strategy, we propose to approximate it by the tangent to the transition point. By means of this strategy, the dissipated energy Ψ_{CD}^{crack} is more accurately estimated, although it cannot be exactly computed. Again, as in [12], the accuracy of this strategy increases considerably if the crack is activated at a later stage of the failure process.

3.2 Crack direction

There are many models which allow to predict the direction of crack growth, mainly based on the stress intensity factors. Nevertheless, since linear elastic fracture mechanics cannot be used in a regularised continuum, different strategies should be developed. Some of these strategies are the ones employed in [11] and [12]. In the former approach, the discontinuity propagates according to the direction of maximum accumulation of the non-local equivalent strain. In the latter, the crack follows the direction of maximum curvature of the damage profile. That is, mechanical criteria are used to define the crack growth.

Here, a new strategy to determine the crack direction is proposed: the discontinuity is propagated following the direction dictated by the medial axis of the damaged domain.

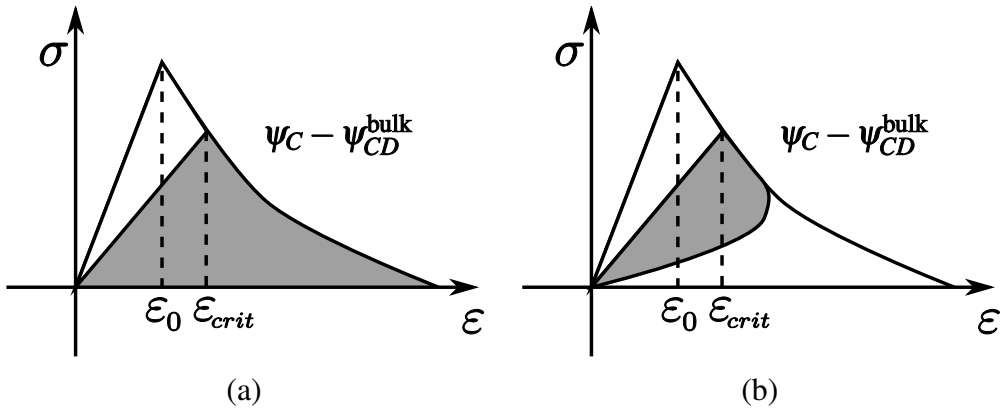

Figure 4: Energy not yet dissipated in the damage band which is transmitted to the cohesive crack and is dissipated by the continuous-discontinuous model, considering that by the continuous strategy, (a) all the points of λ_D download following the softening branch and (b) points of λ_D download following both softening and elastic branches.

3.2.1 The medial axis (MA) and the $\theta-$simplified medial axis ($\theta-$SMA)

The medial axis (MA) of a solid was first proposed by Blum [17] as a geometric tool in image analysis. Intuitively, the MA of an object can be thought of as its skeleton. Mathematically, the MA of a 2D polygon (or the medial surface in a 3D object) may be defined as the loci of centres of bi-tangent interior circles (or spheres), see Figure 5(a).

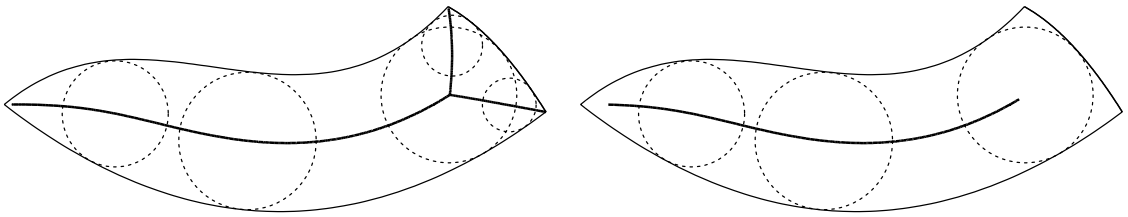

Figure 5: (a) MA of a 2D object; (b) $\theta-$SMA of a 2D object with $\theta = \frac{2\pi}{3}$.

Although this geometric tool is widely used in computer image analysis or for mesh generation purposes, the computation of the MA is a difficult task due to its instability, since it is heavily sensitive to details in the boundary of the object. In order to overcome this main drawback, different simplified and stable versions of the MA can be found in the literature, see [18] for a detailed survey.

One of these stable criteria is based on the separation angle, see [15]. For a point P, the separation angle of this point $S(P)$ may be computed as

$$S(P) = \max(\angle P_1 P P_2) \tag{31}$$

where P_1 and P_2 are the points of tangency of the circle with centre at P to the object, see Figure 6.

Therefore, and given an angle $\theta \in [0, \pi]$, the $\theta-$SMA of an object is defined as the set of points of the MA with separation angle greater than θ, see Figure 5(b).

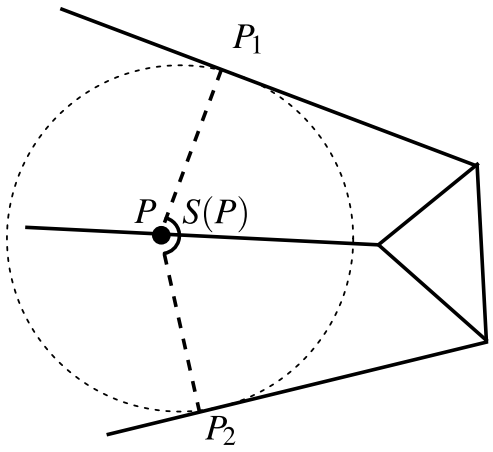

Figure 6: Separation angle $S(P)$ of a point P: adapted from [15].

3.2.2 The $\theta-$SMA as a tool to locate cracks

Once the transition criterion is fulfilled, a propagating crack should be introduced. The proposed strategy consists of different steps:

- Crack initiation: as done in [19], we will assume that a crack may start only from the boundary of the structure. Therefore, once the transition criterion is reached, the boundary element with a highest damage value (D_{crit}) is cracked, thus fixing the damage parameter in this element to D_{crit} and unloading the bulk material, see Figure 7a.

- $\theta-$SMA computation: in order to define the direction of this crack, the $\theta-$SMA of the already damaged domain is computed, see Figure 7b. Note that θ should be large enough in order to avoid the spurious cracks emanating from the main crack (with $\theta > \frac{2\pi}{3}$ only the main path is typically obtained).

- Crack propagation: once the crack tip is located and the $\theta-$SMA is computed, the crack propagation may be defined. The discontinuity goes from the crack tip following the direction dictated by the $\theta-$SMA until $D > D_{\text{crit}}$ is no longer satisfied, see Figure 7c. Note that in order to preserve the robustness of the Newton-Raphson method, this crack is introduced in each finite element as a straight segment at the end of a time step.

- Finite element enrichment: to model a crack tip, the displacement jump at the discontinuity tip is set to zero. In order to prevent crack opening and sliding at the current crack tip, only standard degrees of freedom for the nodes of the edge containing the crack tip are considered, see Figure 7d. As soon as the discontinuity is extended to the next element, nodes behind the crack tip are enriched.

4 APPLICATION TO A THREE-POINT BENDING TEST

A benchmark test such as a three-point bending test has been considered to check the proposed methodology. The test geometry is shown in Figure 8. As seen, a weakened region is considered in order to cause localisation.

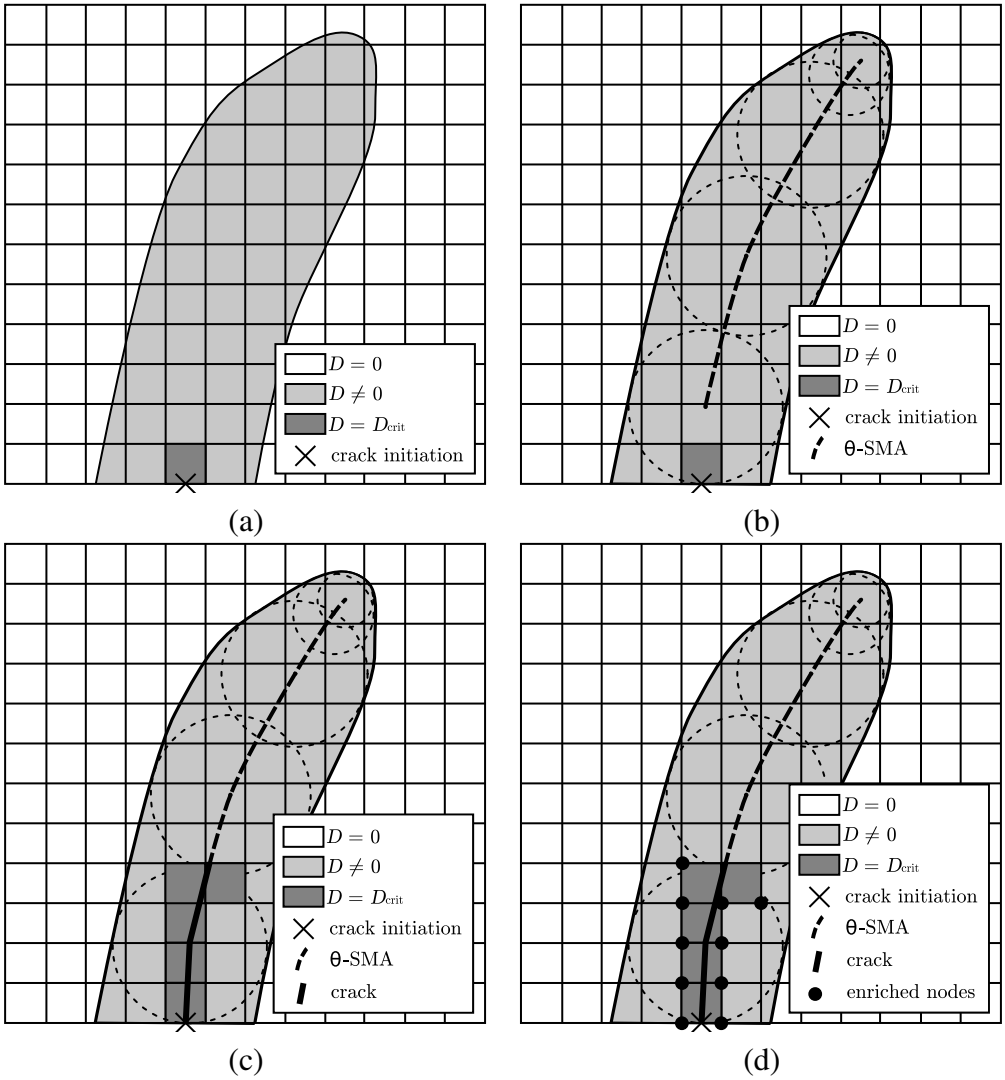

Figure 7: The $\theta-$SMA as a tool to locate cracks: (a) Crack initiation; (b) $\theta-$SMA computation; (c) Crack propagation; (d) Finite element enrichment.

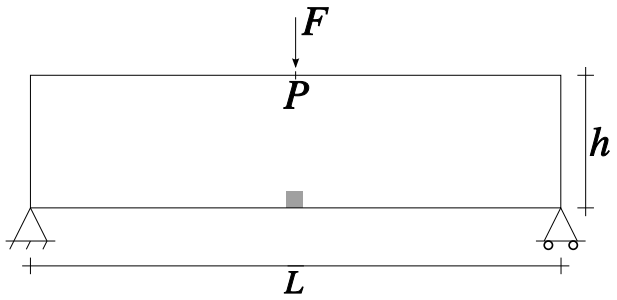

Figure 8: Three-point bending test: problem statement.

A simplified Mazars model with the trilinear softening law

$$D = \begin{cases} 0 & if \quad 0 \leq Y \leq Y_0 \\ \frac{Y_f}{Y_f - Y_0}\left(1 - \frac{Y_0}{Y}\right) & if \quad Y_0 \leq Y \leq Y_f \\ 1 & if \quad Y_f \leq Y \end{cases} \tag{32}$$

are assumed. Based on this damage evolution, the linear traction-separation law

$$\bar{\mathbf{t}}_d = \left\{ \begin{array}{c} \bar{t}_n \\ \bar{t}_s \end{array} \right\} = \mathbf{T} \left\{ \begin{array}{c} [\![\boldsymbol{u}]\!]_n \\ [\![\boldsymbol{u}]\!]_s \end{array} \right\} + \left\{ \begin{array}{c} t_{crit} \\ 0 \end{array} \right\} = \left(\begin{array}{cc} T & 0 \\ 0 & 0 \end{array} \right) \left\{ \begin{array}{c} [\![\boldsymbol{u}]\!]_n \\ [\![\boldsymbol{u}]\!]_s \end{array} \right\} + \left\{ \begin{array}{c} t_{crit} \\ 0 \end{array} \right\} \tag{33}$$

is prescribed, where imposing energy balance, T is obtained.

The geometric and material parameters for this test are summarised in Table 1.

Table 1: Three-point bending test: geometric and material parameters.

Meaning	**Symbol**	**Value**
Length of the specimen	L	3 mm
Width of the specimen	h	1 mm
Young's modulus	E	30 000 MPa
Idem of weaker part	E_W	27 000 MPa
Damage threshold	Y_0	10^{-4}
Final strain	Y_f	1.25×10^{-2}
Poisson's coefficient	ν	0.0

Results are shown in Figure 9. On the one hand, the force-displacement curves are plotted in Figure 9(a). For comparison purposes, both the C and the CD results are shown. As can be seen, the force-displacement curves are completely overlapped thus meaning that the transition is made in such a way that the energy dissipation remains constant. On the other hand, the final damage profile and the deformed mesh are plotted. As seen, the crack propagates following the MA of the damaged domain. Since this profile is regularised, it does not depend on the finite element mesh thus leading to a crack path which is completely independent of numerical parameters.

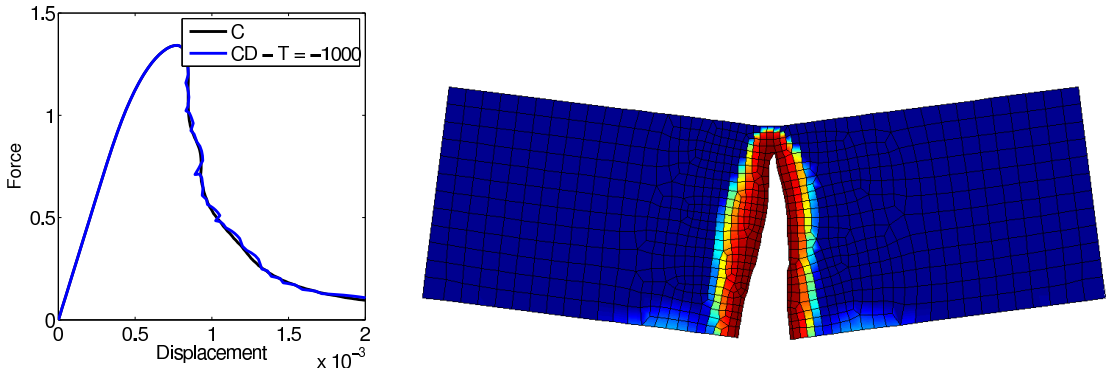

(a) (b)

Figure 9: Three-point bending test: (a) Force-displacement curves obtained with C and CD models; (b) Damage profile with deformed mesh ($\times$ 100).

5 CONCLUDING REMARKS

A combined strategy to simulate failure is proposed. In order to simulate the first stages of the process, a gradient-enriched formulation based on smoothed displacements is employed. Combined boundary conditions are prescribed for the regularisation equation.

Once the transition criterion is fulfilled, this non-local model is enhanced with a discontinuous interpolation of the problem fields in order to describe the final stages of the failure process, where macroscopic cracks can arise. Here, and for consistency purposes, both mechanical and smooth displacements are considered to be discontinuous.

When dealing with these combined strategies, special emphasis should be placed on the transition:

- The cohesive law is defined through an energy balance: the energy remaining to be dissipated by the continuum approach is transmitted to the cohesive zone.
- The evolving cracks propagate across the bulk according to the direction determined by the already damage profile. Particularly, a geometric tool is used. Note that since the damaged bulk is regularised, this profile does not depend on numerical parameters, this leading to a crack path completely independent of the mesh.

By now, some benchmark tests such as a three-point bending test have been carried out and more research is still needed in order to generalise the applicability of this new methodology.

REFERENCES

[1] J. Lemaitre, J.L. Chaboche: Mechanics of solid materials. Cambridge University Press, 1990.

[2] J. Mazars, G. Pijaudier-Cabot: From damage to fracture mechanics and conversely: a combined approach. *International Journal of Solids and Structures*, 33 (1996), 3327–3342.

[3] M. Jirásek: Mathematical analysis of strain localization. *Revue Européenne de Génie Civil*, 11 (2007), 977–991.

[4] M. Jirásek: Nonlocal damage mechanics. *Revue Européenne de Génie Civil*, 11 (2007), 993–1021.

[5] A. Hillerborg, M. Modeer, P.A. Petersson: Analysis of crack formation and crack growth in concrete by means of fracture mechanics and finite elements. *Cement and Concrete Research*, 6 (1976), 773–782.

[6] M. Jirásek, T. Belytschko: Computation Resolution of Strong Discontinuities. In *Fifth World Congress on Computational Mechanics*, 2002.

[7] T. Belytschko, T. Black: Elastic crack growth in finite elements with minimal remeshing. *International Journal for Numerical Methods in Engineering*, 45 (1999), 601–620.

[8] N. Moës, J. Dolbow, T. Belytschko: A finite element method for crack growth without remeshing. *International Journal for Numerical Methods in Engineering*, 46 (1999), 131–150.

[9] M. Jirásek, T. Zimmermann: Embedded crack model: II. Combination with smeared cracks. *International Journal for Numerical Methods in Engineering*, 50 (2001), 1291–1305.

[10] G.N. Wells, L.J. Sluys, R. de Borst: Simulating the propagation of displacement discontinuities in a regularized strain-softening medium. *International Journal for Numerical Methods in Engineering*, 53 (2002), 1235–1256.

[11] A. Simone, G.N. Wells, L.J. Sluys: From continuous to discontinuous failure in a gradient-enhanced continuum damage model. *Computer Methods in Applied Mechanics and Engineering*, 192 (2003), 4581–4607.

[12] C. Comi, S. Mariani, U. Perego: An extended FE strategy for transition from continuum damage to mode I cohesive crack propagation. *International Journal for Numerical and Analytical Methods in Geomechanics*, 31 (2007), 213–238.

[13] A. Rodríguez-Ferran, I. Morata, A. Huerta: A new damage model based on non-local displacements. *International Journal for Numerical and Analytical Methods in Geomechanics*, 29 (2005), 473–493.

[14] A. Rodríguez-Ferran, T. Bennett, H. Askes, E. Tamayo-Mas: A general framework for softening regularisation based on gradient elasticity. *International Journal of Solids and Structures*, 48 (2011), 1382–1394.

[15] M. Foskey, M.C. Lin, D. Manocha: Efficient Computation of a Simplified Medial Axis. *Journal of Computing and Information Science in Engineering*, 3 (2003), 274–284.

[16] E. Tamayo-Mas, A. Rodríguez-Ferran: Condiciones de contorno en modelos de gradiente con desplazamientos suavizados, Revista Internacional de Métodos Numéricos para Cálculo y Diseño en Ingeniería (2012) doi:10.1016/j.rimni.2012.03.006.

[17] H. Blum: A transformation for extracting new descriptors of shape. In *W. Wathen-Dunn, editor, Models for the Perception of Speech and Visual Form*, (1967), 362–380.

[18] S.M. Pizer, K. Siddiqi, G. Szekely, J.N. Damon, S.W. Zucker: Multiscale Medial Loci and Their Properties. *International Journal of Computer Vision*, 55 (2003), 155–179.

[19] M. Cervera, L. Pela, R. Clemente, P. Roca: A crack-tracking technique for localized damage in quasi-brittle materials. *Engineering Fracture Mechanics*, 77 (2010), 2431–2450.

[20] F. Cazes, M. Coret, A. Combescure, A. Gravouil: A thermodynamic method for the construction of a cohesive law from a nonlocal damage model. *International Journal of Solids and Structures*, 46 (2009), 1476–1490.